Research Square

Preprints are preliminary reports that have not undergone peer review.
They should not be considered conclusive, used to inform clinical practice,
or referenced by the media as validated information.

ZNF460–SNRPB–RDM1 Splicing Axis Drives Genomic Instability and Therapeutic Vulnerability in Clear Cell Renal Cell Carcinoma

Liu Kang
The Second Affiliated Hospital of Soochow University
Yao Yao
The Second Affiliated Hospital of Soochow University
Xiang Han
The Second Affiliated Hospital of Soochow University
Wang Yang
The Second Affiliated Hospital of Soochow University
Jiang Chunchao
The Second Affiliated Hospital of Soochow University
Wang Lixia
The Second Affiliated Hospital of Soochow University
Zhu Jin
oceanzhu79@qq.com
The Second Affiliated Hospital of Soochow University

Research Article

Keywords: Renal clear cell carcinoma, SNRPB:RDM1:Alternative splicing, Genomic instability, ZNF460

Posted Date: September 17th, 2026

DOI: https://doi.org/10.21203/rs.3.rs-10842124/v1

License: This work is licensed under a Creative Commons Attribution 4.0 International License.
Read Full License

Additional Declarations: No competing interests reported.

ZNF460–SNRPB–RDM1 Splicing Axis Drives Genomic Instability and Therapeutic Vulnerability in Clear Cell Renal Cell Carcinoma

Liu Kang*[1], Yao Yao*[1], Xiang Han*[1], Wang Yang[1], Jiang Chunchao[1], Wang Lixia[1] and Zhu Jin[1]

Corresponding author: Wang Lixia and Zhu Jin

[1]Department of Urology, The Second Affiliated Hospital of Soochow University, Suzhou, China.

Abstract

Small nuclear ribonucleoprotein polypeptide B (SNRPB) is one of the core proteins of the spliceosome. Although its role in spliceosome assembly has been well - established, its carcinogenic potential has just begun to be revealed. We found that its expression is significantly increased in clear cell renal cell carcinoma (ccRCC) and is associated with a poor prognosis. Mechanistically, this study reveals a carcinogenic axis centered around abnormal RNA splicing: the ZNF460–SNRPB–RDM1 axis. The upstream transcription factor ZNF460 directly binds to and activates the SNRPB promoter, leading to the abnormally high expression of the core spliceosome protein SNRPB in ccRCC. Excessive SNRPB interferes with the precise splicing of RDM1 pre - mRNA, resulting in the dysregulated expression of functional RDM1 protein. As a key effector molecule in the homologous recombination repair (HRR) pathway, changes in the expression level of RDM1 alter the sensitivity of ccRCC cells to the PARP inhibitor olaparib. Therefore, this axis is not only a newly discovered driver of ccRCC invasiveness and drug resistance but may also be a new therapeutic target.

Keywords: Renal clear cell carcinoma; SNRPB:RDM1:Alternative splicing; Genomic instability; ZNF460

Introduction

Globally, kidney cancer is the 14th most common cancer(1), with clear cell renal cell carcinoma (ccRCC) accounting for approximately 75%–80% of all cases(2). Although targeted therapies and immunotherapies such as tyrosine kinase inhibitors (TKIs) like sunitinib, and immune checkpoint inhibitors (ICIs) have significantly improved the survival of patients with advanced disease, acquired resistance has become the leading cause of treatment failure and patient death(3, 4). These findings highlight the urgent need to elucidate the novel molecular mechanisms driving the pathogenesis of ccRCC to identify new therapeutic targets.

The pathogenesis of ccRCC is closely related to the loss of the von Hippel–Lindau (VHL) tumor suppressor gene(5), which leads to the continuous activation of the hypoxia-inducible factor (HIF) signaling pathway, thereby promoting angiogenesis and tumor growth(6). However, the VHL–HIF axis alone cannot fully explain the extensive heterogeneity and invasiveness of ccRCC(5, 7, 8), indicating that other carcinogenic pathways are involved. Precursor messenger RNA (pre-mRNA) splicing is a core step in eukaryotic gene expression, and alternative splicing (AS) greatly increases the diversity of the proteome(9). In recent years, numerous studies have demonstrated that widespread dysregulation of pre-mRNA splicing is an emerging hallmark of cancer(10-12). Spliceosome components are often abnormally expressed in various tumors and promote tumorigenesis and tumor development by generating abnormal splicing variants that promote cell proliferation, invasion, and metastasis(13, 14).

Of these components, small nuclear ribonucleoprotein polypeptide B (SNRPB) is among the core proteins of the spliceosome(15). Although its role in spliceosome assembly is well established, its carcinogenic potential has only recently begun to be revealed. SNRPB is highly expressed in

various cancers, where it promotes cell proliferation and tumor growth(15-17). However, its expression pattern, biological functions, and underlying molecular mechanisms in ccRCC remain incompletely understood.

This study aims to comprehensively explore the role of SNRPB in the progression of clear cell renal cell carcinoma (ccRCC). We evaluated the expression level of SNRPB in the tissues of ccRCC patients and correlated it with clinicopathological features. The results revealed that SNRPB was highly expressed in ccRCC tissues and was associated with poor patient prognosis. SNRPB promoted the malignant phenotype of ccRCC cells both in vivo and in vitro. We also revealed that SNRPB affects the effective splicing of RDM1 by regulating exon skipping. Our findings reveal a new oncogenic function of SNRPB in ccRCC. Therefore, SNRPB may be a promising therapeutic target for ccRCC treatment.

Materials and methods

Bioinformatics analysis

This study integrated three types of public data: single - cell transcriptome data were from GEO database GSE156632 (renal cell carcinoma, 13 samples: 7 tumor and 6 paired normal tissues); spatial transcriptome data were from GSM6415705; Bulk RNA - seq data were from TCGA (33 cancer types) and GEO dataset GSE66272 (platform GPL570).

1.Single - cell and spatial transcriptome analysis

Seurat (v5) was used for data analysis. After data were normalized by SCTransform, the Harmony algorithm was used to correct batch effects. A shared nearest neighbor graph was constructed based on PCA dimensionality reduction and visualized by UMAP and t - SNE. Manual annotation was adopted. Based on the differentially expressed genes of each cluster (Wilcoxon rank - sum test, min.pct = 0.25, logfc.threshold = 0.25, only positive markers were retained) and combined with the classic cell - type marker genes of renal tissues, the clustering results were annotated as epithelial cells, fibroblasts, myeloid cells, endothelial cells, T cells, B cells, etc. In tumor samples, cells were divided into High (Detected) and Low (Not Detected) groups according to the expression level of SNRPB, and differential expression analysis (Wilcoxon test) was performed within each cell type. clusterProfiler was used for GO biological process (BP) enrichment analysis (pvalueCutoff = 0.1, qvalueCutoff = 0.2). The spatial transcriptome data (GSM6415705) were normalized by SCTransform. The cell - type labels of single - cell reference data were mapped to spatial sites using the Seurat anchor integration method (TransferData). The cell composition at each spatial location was inferred based on the predicted probability, and the spatial expression distribution of SNRPB was shown by a two - dimensional density contour map.

2.TCGA pan - cancer and renal cell carcinoma cohorts

RNA - seq expression data (in FPKM format) standardized by the STAR process for 33 cancer types and clinical follow - up information were downloaded from the TCGA database (https://portal.gdc.cancer.gov). R (v4.2.1) was used for data processing and visualization. Pan - cancer expression profile radar chart: The Mann - Whitney U test (Wilcoxon rank - sum test) was performed on 33 solid tumors and their paired normal tissues. After the data were transformed by log2(FPKM + 1), the mean difference was calculated. The radar chart was drawn using ggplot2 to show the differential expression patterns of SNRPB in multiple cancers (only statistically significant cancers were shown).

For KIRC tumors and paired normal tissues, box plots were drawn using ggplot2 to show the expression distribution. Survival analysis: Normal samples and cases with missing clinical information were excluded from the TCGA - KIRC cohort. The SNRPB expression data were transformed by log2(FPKM + 1). The Kaplan - Meier method was used to draw survival curves, and the Log - rank test was used to compare the differences between groups.

3.Analysis of GEO dataset GSE66272

The expression values of ZNF460 and SNRPB were extracted, and the Pearson correlation coefficient was used to evaluate their co - expression relationship. The co - expression scatter plot was drawn using ggplot2 and the ggside package, with a linear regression fitting line (95% confidence interval) and marginal density distribution added (the height of the ridgeline plot was set to 12%), and the expression distribution characteristics were shown by coloring according to groups.

4.Statistical analysis

All analyses were completed in the R (v4.3.0) environment. The Wilcoxon rank - sum test or Wilcoxon signed - rank test was used for the comparison of continuous variables; the Pearson or Spearman method was used for correlation analysis; the Benjamini - Hochberg method (FDR) was used for multiple - test correction. The Log - rank test was used for survival analysis, and $P < 0.05$ was considered to indicate a statistically significant difference.

Cell Culture

The cell lines used in the study are as follows: 786 - O, 769 - P, CAKI - 1, HK2, and 293T, all purchased from Procell (Wuhan, China). 786 - O cells were cultured in RPMI - 1640 medium (Gibco, USA) containing 10% fetal bovine serum (Gibco, USA). 769 - P, HK2, CAKI - 1, and 293T cells were cultured in DMEM (Gibco, USA) medium containing 10% high - quality fetal bovine serum. All cells were cultured in a humid environment at 37°C with 5% CO_2. The culture medium and supplements were renewed every 2 - 3 days, and cells were passaged when they reached approximately 80% - 90% confluence.

Lentiviral Infection

The shRNA plasmids and helper plasmids psPAX2 and pMD2.G used for lentiviral packaging and production were purchased from Youbao Biotechnology (Changsha, China). They were separately transfected into HEK - 293T cells to produce lentiviruses. 48 - 72 hours after transfection, the lentiviruses in the culture supernatant were collected. 786 - O and 769 - P cells were infected with the lentiviral supernatant, and stable cells were selected with 10 μg/ml puromycin (GenePharma, Shanghai, China). Western blotting analysis was used to determine the gene knockout efficiency.

Cell Viability Assay

The viability of 786 - O and 769 - P cells was determined by the CCK - 8 colorimetric method. After cell treatment, the culture medium in the 96 - well plate was removed, and 100 μL of fresh medium containing 10 μL of CCK - 8 was added to each well. After incubation at 37°C for 1 - 2 h, the absorbance at 450 nm was measured using a microplate reader. For the EDU assay: Cells were seeded in a 24 - well plate. After cell attachment, they were incubated and stained according to the instructions of the EDU proliferation kit (Beyotime, USA), and then the absorbance at 450 nm was measured

using a microplate reader.

Apoptosis Rate Assay

The apoptosis rate of cells was detected using the Annexin V/PI kit (Lianke Biotechnology, China). After cell treatment, cells were washed with pre - cooled PBS and resuspended in 500 μl of binding buffer. They were stained with PI and Annexin V - FITC for 5 min at room temperature. The apoptosis of cells was analyzed using a flow cytometer (Beckman, Germany).

Wound Healing Assay

Cells were seeded in a 6 - well plate. When the cells grew to nearly 95% confluence, the cells were scratched with the tip of a 200 - μl pipette. Images were captured at 0 h and 24 h, respectively. It was observed that the cells at the edge of the wound scratch gradually migrated into the gap, and the scratch observed under the optical microscope gradually healed. ImageJ was used to quantify the cell migration rate.

Invasion Ability Assay

A Transwell chamber (Corning, USA) was pre - coated with Matrigel (Corning, USA, diluted 1:8 in serum - free medium) at 37°C for 30 min to evaluate the cell invasion ability. After the cells were starved for 24 hours, they were seeded in the upper chamber, and 500 μl of medium containing 10% fetal bovine serum was used as a chemotactic reagent in the lower chamber. After incubation in a 37°C incubator for 24 hours, the cells that migrated to the bottom were fixed with 4% paraformaldehyde for 15 minutes. Subsequently, they were stained with crystal violet for 15 minutes, and the cells in three randomly selected fields were counted under a microscope.

Experimental Study of Subcutaneous Xenograft Tumors in Nude Mice

Six - week - old female BALB/c nude mice (Shanghai SLAC Laboratory Animal Co., Ltd., China) were divided into three groups: shNC, shSNRPB, and shSNRPB + oe - RDM1, and were subjected to xenotransplantation of the corresponding cells. The cells were injected subcutaneously into the mice. The volume of subcutaneous tumors was measured every 5 days, and the calculation formula was: Tumor volume = $0.52 \times a \times b^2$ (a: maximum diameter of the tumor, b: minimum diameter of the tumor). On the 25th day, the mice were sacrificed by cervical dislocation, and the tumors were collected. All animal experiments were approved by the Animal Experiment Ethics Committee of Soochow University.

Dual - Luciferase Reporter Assay

In this study, a dual - luciferase reporter experiment was conducted to study the transcriptional activity of ZNF460 on the SNRPB promoter. The wild - type SNRPB promoter or mutant was cloned into the pGL3 - luciferase reporter vector (Youbao, China). Mutations were introduced at specific positions in the SNRPB promoter to evaluate the effect of ZNF460 binding on promoter activity. The reporter vector was - co transfected with the ZNF460 overexpression vector or control vector into cells using Lipofectamine 3000 (Thermo Fisher Science, USA). After 48 h of incubation, the cells were lysed to extract the components required for analysis. The luciferase activity was detected using a dual - luciferase reporter analysis system (Promega, USA).

Quantitative Polymerase Chain Reaction (qPCR)

Total RNA from cultured cells was extracted using TRIzol reagent (Invitrogen). To synthesize cDNA, reverse transcription was performed using the Revertaid RT Kit

(Thermo Fisher Science, USA). Quantitative polymerase chain reaction (qPCR) was performed using SYBR Green Mix (NovoProtein, China). The gene expression levels were normalized to the internal reference gene β - ACTIN and calculated using the $2^{-\Delta\Delta Ct}$ method.

Western Blotting Analysis

Cells were lysed with pre - cooled RIPA lysis buffer (Beyotime, USA) to extract proteins. Protein quantification was performed using a BCA protein quantification kit (Beyotime, USA). Proteins were separated by SDS - PAGE and then transferred to a nitrocellulose (NC) membrane. After the samples were blocked with 5% non - fat milk at room temperature for 1 h, they were incubated with the primary antibody overnight at 4°C and then with the appropriate secondary antibody at room temperature for 1 h. Protein bands were visualized using OMNI - ECL™ reagent (YEASEN, Shanghai, China).

Immunohistochemical (IHC) Staining

The tissues in this study were obtained from newly diagnosed clear - cell renal cell carcinoma patients in the Department of Urology of the Second Affiliated Hospital of Soochow University, with the informed consent of the patients. This study was approved by the Ethics Committee of the Second Affiliated Hospital of Soochow University (JD - LK2024067I01), and written informed consent was obtained from each patient or their legal guardian. Human KIRC tissue and normal tissue microarrays were from Aifang Biotechnology Co., Ltd. (Changsha, Hunan, China). The final score of each sample was determined based on the staining intensity and degree on the section.

Results

Upregulated expression of SNRPB is associated with poor prognosis in clear cell renal cell carcinoma (KIRC)

We analyzed data from the TCGA database to investigate the predictive role of SNRPB in KIRC. Compared with that in normal renal tissues, the expression of SNRPB was significantly higher in tumor tissues (Figure 1A–B). Kaplan–Meier survival curve analysis revealed that low SNRPB expression was associated with better prognosis in KIRC patients (Figure 1C). In addition, data from the TCGA database revealed that the expression of SNRPB was related to various clinical features, such as tumor stage, tumor progression, overall survival, disease-specific survival, and progression-free interval events (Table 1). Immunohistochemical (IHC) staining of tumor tissues from 70 KIRC patients further confirmed that the expression of SNRPB was significantly higher in tumor tissues than in paired normal tissues (Figure 1D–E). Notably, the expression of SNRPB in 3 human renal cancer cell lines was higher than that in the human renal tubular epithelial cell line HK-2 (Figure 1F–G). Western blotting analysis of protein samples collected from KIRC patients also revealed that the expression of SNRPB was upregulated in KIRC tissues compared with paired normal tissues (Figure 1H). In conclusion, the aforementioned data indicate that the expression of SNRPB is upregulated in KIRC and that upregulated SNRPB expression is associated with poor prognosis in patients.

Fig1

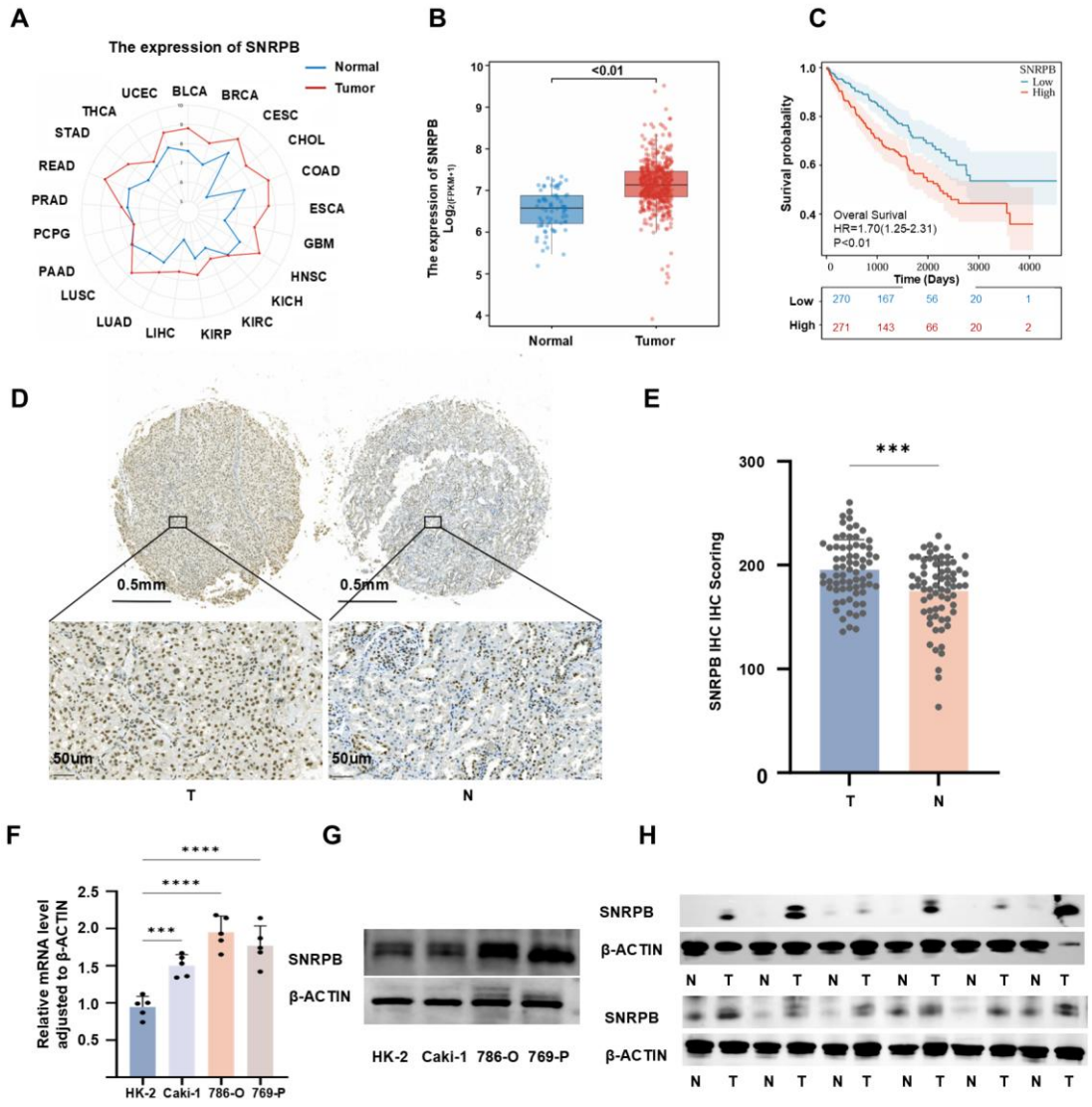


Figure 1. Upregulated expression of SNRPB in clear cell renal cell carcinoma (KIRC) is associated with poor prognosis. **A:** Expression of the SNRPB gene in tumor tissues and matched normal tissues of different tumor types in the TCGA database. **B:** Expression of SNRPB mRNA in KIRC. **C:** Kaplan–Meier survival curves of SNRPB in KIRC patients. **D–E:** Representative IHC staining and SNRPB expression scores in 70 KIRC specimens and paired paracancerous specimens. Scale bar: 50 μm. **F–G:** RNA and protein expression levels of SNRPB in four cell lines. **H:** Western blot analysis of SNRPB protein expression in 12 fresh KIRC tissues and adjacent normal tissues. ****p < 0.001, ****p < 0.0001*.

Table1

Clinical Characteristics	Low expression of SNRPB (n = 270)	High expression of SNRPB (n = 271)	P value	χ^2 statistic
			0.034	8.70
Pathologic T stage	151 (27.9%)	128 (23.7%)		
	37 (6.8%)	34 (6.3%)		
	80 (14.8%)	100 (18.5%)		
	2 (0.4%)	9 (1.7%)		
			0.458	0.55
Pathologic N stage	129 (50.0%)	113 (43.8%)		
	7 (2.7%)	9 (3.5%)		
			0.001	10.48
Pathologic M stage	237 (46.7%)	192 (37.8%)		
	28 (5.5%)	51 (10.0%)		
			0.011	11.24
Pathologic stage	148 (27.5%)	125 (23.2%)		
	34 (6.3%)	25 (4.6%)		
	58 (10.8%)	65 (12.1%)		
	29 (5.4%)	54 (10.0%)		
			< 0.001	13.98
OS event	203 (37.5%)	163 (30.1%)		
	67 (12.4%)	108 (20.0%)		
			< 0.001	22.54
DSS event	231 (43.6%)	190 (35.8%)		
	32 (6.0%)	77 (14.5%)		
			< 0.001	15.32
PFI event	210 (38.8%)	169 (31.2%)		
	60 (11.1%)	102 (18.9%)		

Table 1. The expression of SNRPB is associated with various clinical features.

Analysis of cell-specific and spatially heterogeneous SNRPB expression in the tumor microenvironment of clear cell renal cell carcinoma (ccRCC)

UMAP visualization showed six major cell populations, including epithelial cells, T cells, myeloid cells, B cells, fibroblasts, and endothelial cells (Figure 2A). DotPlot validated the expression specificity of markers for each cell type: markers for B cells (CD79A, CD79B, MS4A1), myeloid cells (CD14, CD68, LYZ), fibroblasts (COL1A1, COL1A2, DCN), epithelial cells (EPCAM, KRT8, KRT18), endothelial cells (PECAM1, VWF, CDH5), and T cells (CD3D, CD3E, IL7R) all showed obvious cell type-restricted expression patterns (Figure 2B). The UMAP faceted plot showed distribution the of cell populations of SNRPB in tumor and normal tissues (Figure 2C). SNRPB was widely expressed in various cells. The ridgeline density plot showed that the overall expression distribution of SNRPB in each cell type in the tumor group shifted to the right. Among them, the inter-group differences in epithelial cells, myeloid cells, and T cells were relatively obvious (Figure 2D, left). Detection rate analysis showed that the proportion of SNRPB-positive cells in tumor tissues was higher than that in normal tissues in most cell types, and the detection rates in epithelial cells, T cells, and myeloid cells in tumor tissues were the highest; the detection rate of fibroblasts in tumors (26.3%) was slightly lower than that in normal tissues (31.8%) (Figure 2D, right). In tumor samples, differential expression analysis was performed by grouping according to the expression level of SNRPB. GO enrichment analysis showed that in epithelial cells, SNRPB-related genes were mainly enriched in the establishment of protein localization and

energy metabolism; in myeloid cells, they were involved in RNA splicing and ribosome biogenesis; in fibroblasts, they were related to vesicle transport and endoplasmic reticulum stress (Figure 2E).Based on the TCGA-KIRC cohort, the expression of SNRPB was significantly negatively correlated with the infiltration of CD8+ T cells, M0 macrophages, and regulatory T cells (Tregs) (FDR < 0.05), suggesting that high expression of SNRPB may be accompanied by an immunosuppressive microenvironment (Figure 2F). After SCTransform normalization of the spatial transcriptome data (GSM6415705), the single-cell reference data were mapped to spatial sites using the Seurat anchor integration method. H&E staining of tissue sections showed the tissue structure of the tumor area (Figure 2G, left). The spatial distribution map of cell types showed that each cell type was regionally distributed in the tissue section (Figure 2G, middle). The spatial map of SNRPB expression showed that it was highly expressed in the regions of myeloid cells and T cells (Figure 2g, right).

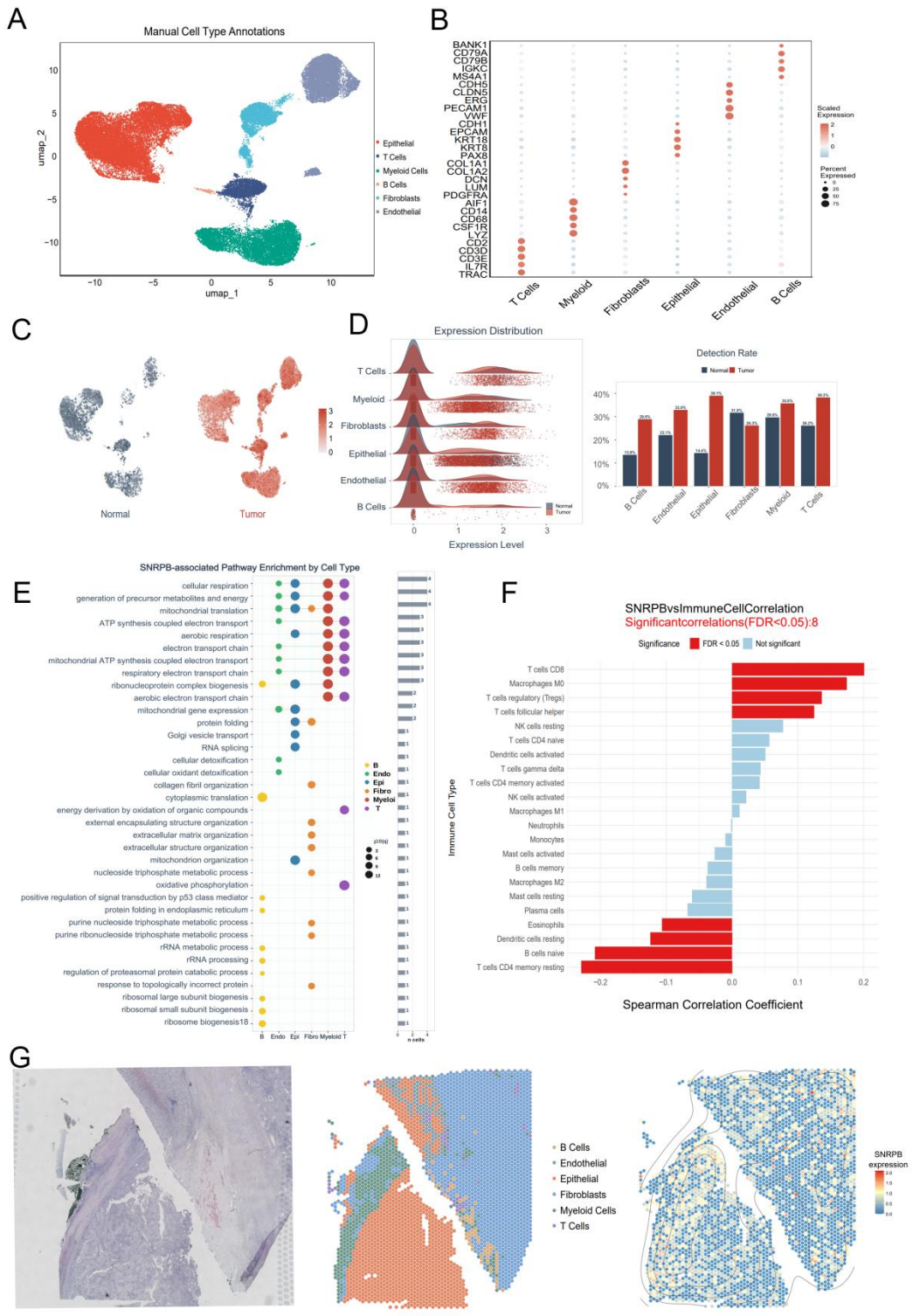


Figure 2 Construction of a single-cell atlas of renal cell carcinoma and analysis of SNRPB expression characteristics. **A:** UMAP dimensionality reduction visualization of single-cell data from 13 renal cell carcinoma samples (7 tumors and 6 paired normal tissues), showing 6 major cell types identified by manual annotation.**B:** Bubble plot of the expression profiles of cell type marker genes. The x–axis represents cell types, and the y–axis represents marker genes; the color intensity indicates the standardized expression

level (Z–score), and the dot size indicates the proportion of cells with gene expression. **C:** Diagram of the expression distribution characteristics of SNRPB at the single - cell level. The left side shows normal tissues, and the right side shows tumor tissues. The color intensity represents the expression intensity.**D:** Left: A ridgeline density plot showing the distribution differences of SNRPB expression levels between normal (blue) and tumor (red) groups in each cell type; Right: A bar chart comparing the differences in the positive detection rates of SNRPB in different cell types between normal and tumor samples.**E:** Bubble plot of the enrichment analysis of SNRPB–related pathways. It shows the GO biological processes enriched by the differentially expressed genes between the high–and low–SNRPB expression groups in different cell types such as epithelial cells, fibroblasts, and myeloid cells; the bubble size represents - log10(q - value), the colors distinguish different cell types, and the bar chart on the right shows the frequency of the pathway common to several cell types.**F:** Based on the TCGA-KIRC cohort, SNRPB expression was significantly positively correlated with the infiltration of CD8+ T cells, M0 macrophages, regulatory T cells (Tregs), and follicular helper T cells (Tfh) (FDR < 0.05), while it was significantly negatively correlated with the infiltration of resting CD4 memory T cells, naive B cells, resting dendritic cells, and eosinophils (FDR < 0.05).**G:** Spatial transcriptome analysis. Left: H&E staining of tissue sections; Middle: Spatial distribution of cell types mapped based on single - cell reference data; Right: Contour map of the spatial distribution of SNRPB expression, with warm colors indicating high–expression regions.

SNRPB promotes the in vitro progression of clear cell renal cell carcinoma

To investigate the functional role of SNRPB in clear cell renal cell carcinoma, 786-O and 769-P cells with relatively high endogenous SNRPB expression were selected for loss-of-function studies. shRNAs (Figure S1C) targeting SNRPB were designed, and the knockdown efficiency was further verified at the mRNA and protein levels (Figure 3A, Figure S1A). Moreover, a plasmid overexpressing SNRPB was constructed and verified in cells (Figure 3B, Figure S1B). A functional analysis was subsequently performed to evaluate the effect of SNRPB gene knockout on the phenotype of clear cell renal cell carcinoma cells. The results of the CCK-8 assay revealed that, compared with the shNC group, the proliferation of clear cell renal cell carcinoma cells was significantly reduced after SNRPB was silenced (Figure 3C), while overexpression of SNRPB significantly increased the proliferation of 786-O and 769-P cells (Figure 3D). The results of the EDU experiments further confirmed these results (Figure 3E–F). The invasion and migration abilities of cells after SNRPB gene knockout were analyzed using Transwell (Figure 3G–H) and wound healing assays (Figure 3I–J, Figure S1E–F). The results revealed that the invasion and migration abilities of clear cell renal cell carcinoma cells were significantly decreased, whereas overexpression of SNRPB significantly enhanced these abilities. Flow cytometry was performed to assess apoptosis and investigate the effect of SNRPB expression on cell survival. SNRPB gene knockout significantly increased the apoptosis rates of 786-O and 769-P cells, whereas SNRPB overexpression had the opposite effect (Figure 3K–M, Figure S1G–H).

Fig3

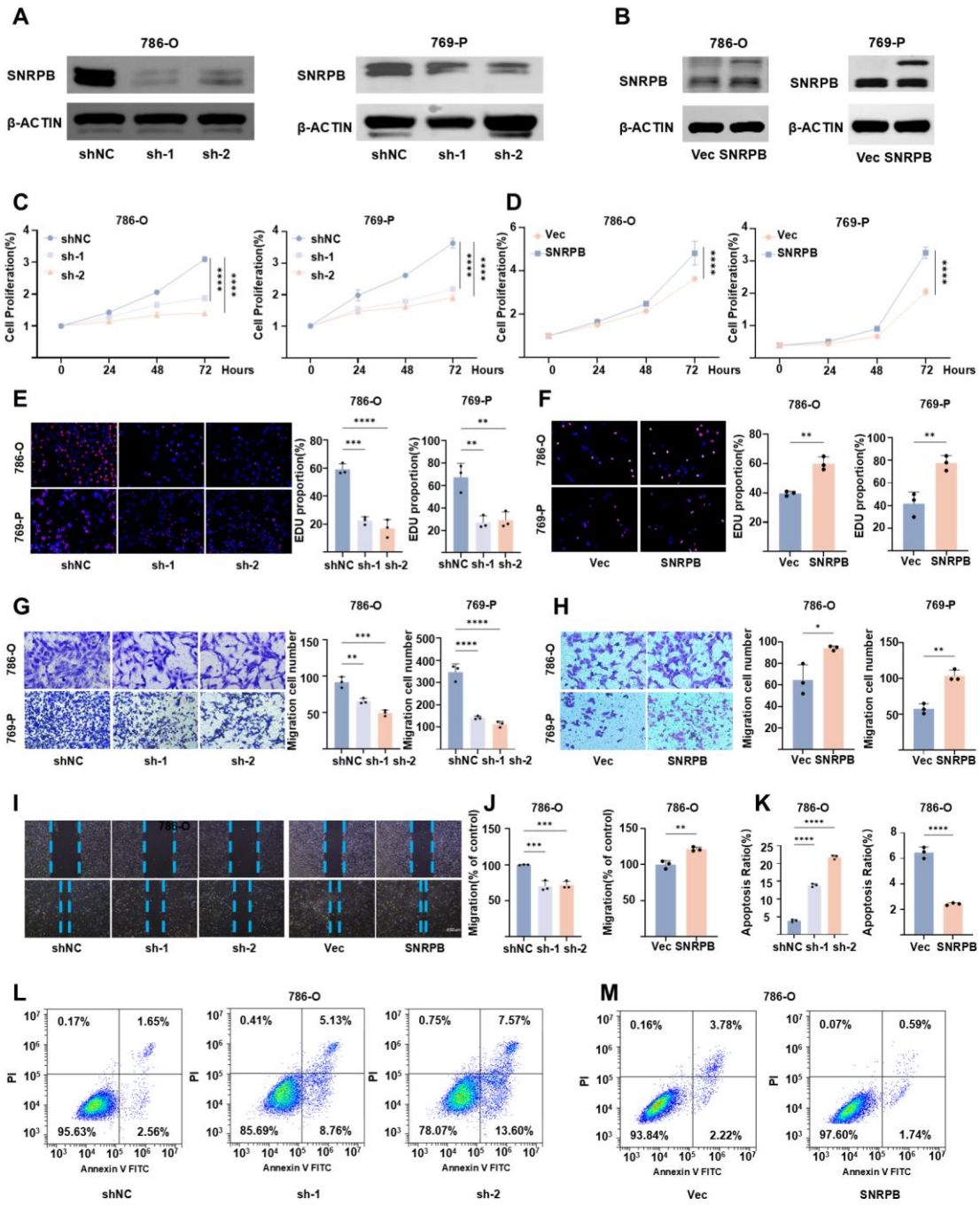


Figure 3. SNRPB silencing inhibits the proliferation and motility of clear cell renal carcinoma cells in vitro. **A–B:** Western blotting to verify the knockdown and overexpression efficiency of SNRPB in 786–O and 769–P cells. **C–D:** Detection of the effect of SNRPB knockdown and overexpression on cell viability by the CCK - 8 assay. **E–F:** EDU assay to detect the effect of SNRPB knockdown and overexpression on cell proliferation. **G–H:** Transwell assay to detect the effect of SNRPB knockdown and overexpression on the invasion ability of clear cell renal carcinoma cells. **I–J:** Scratch test to detect the effect of SNRPB knockdown and overexpression on the migration ability of

786–O cells. **K–M:** Flow cytometry to quantitatively detect the effect of SNRPB knockdown and overexpression on the apoptosis rate of 786 - O cells. ***p < 0.01, ***p < 0.001, ****p < 0.0001*.

The transcription factor ZNF460 mediates the transcriptional activation of SNRPB

Previous studies have shown that SNRPB plays an important role in the progression of clear cell renal cell carcinoma. Therefore, we attempted to identify its upstream transcription factor. First, using the JASPAR database for prediction, we identified the transcription factor ZNF460 (Figure 4A, Figure S1D). Bioinformatics analysis revealed a positive correlation between ZNF460 and SNRPB (Figure 4B). We knocked down and overexpressed ZNF460 in 786-O and 769-P cells. The results revealed that silencing ZNF460 significantly downregulated the expression of SNRPB and that overexpressing ZNF460 significantly promoted the transcription of SNRPB (Figure 4C–F). We further predicted the binding sites of ZNF460 and the SNRPB promoter region by referring to the JASPAR database (Figure 4G). We hypothesized that ZNF460 is a transcription factor of SNRPB and conducted a dual-luciferase reporter gene assay. The results showed that silencing ZNF460 significantly inhibited the activity of SNRPB luciferase (Figure 4H) and that overexpressing ZNF460 significantly promoted the activity of SNRPB luciferase SNRPB (Figure 4I). After the sequence of the SNRPB promoter region that may interact with ZNF460 was mutated (Figure 4J), the transcriptional activation effect of ZNF460 on SNRPB was significantly reduced (Figure 4K), indicating that ZNF460 exerts its function at this site.

Fig4

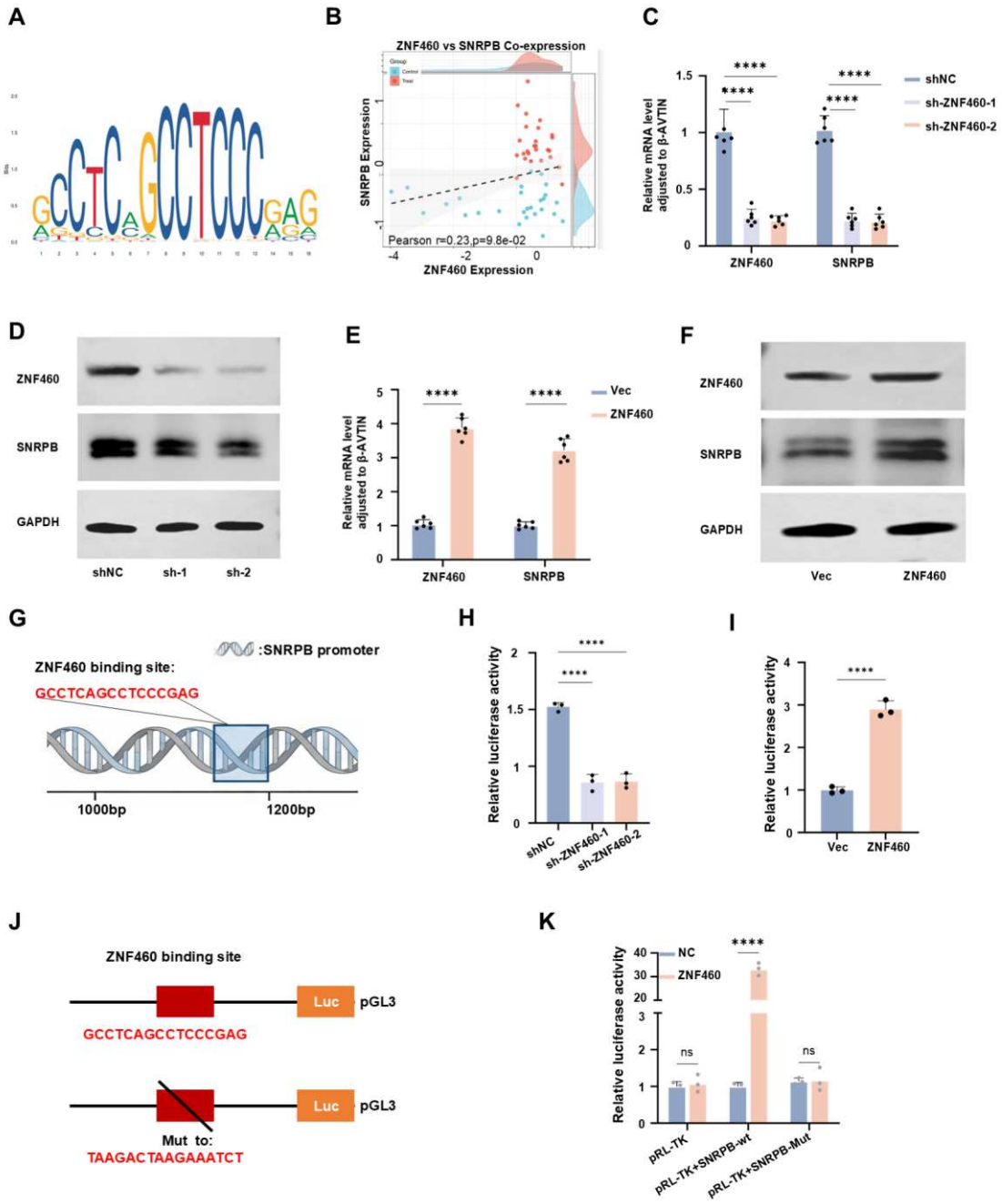


Figure 4. ZNF460 promotes SNRPB transcription by binding to a specific sequence in the SNRPB promoter. **A:** Sequence diagram of the ZNF460 binding site predicted by the JASPAR website. **B:** Analysis of the correlation between ZNF460 and SNRPB expression in KIRC patients from the GSE66272 dataset. **C–F:** Detection of ZNF460 and SNRPB protein and mRNA levels after knockdown and overexpression of ZNF460 in 786 - O cells. G: Schematic diagram of the potential ZNF460 binding site in the SNRPB promoter. **H–I:** The full–length SNRPB promoter luciferase gene was introduced into 786–O/shZNF460 cells and 780–O/ZNF460 cells. Transcriptional activation was analyzed by the dual–

luciferase reporter assay. **J:** Mutation of the 16–base sequence of the potential ZNF460 binding site in the SNRPB promoter. **K:** The luciferase vector of the wild - type or mutant SNRPB promoter was introduced into 780–O/ZNF460 cells. The results were normalized to Renilla luciferase activity and expressed as the fold–change in luciferase activity relative to the control. ****$p < 0.0001$.

SNRPB regulates RDM1 expression through alternative splicing

To investigate the mechanism by which SNRPB promotes the malignant biological behavior of clear cell renal cell carcinoma (ccRCC) cells, we performed RNA-seq on RNA samples from SNRPB-silenced 786-O cells and control cells to analyze differentially expressed genes (DEGs). Through differential expression analysis, we identified a total of 824 upregulated genes and 1151 downregulated genes (Figure 5A). KEGG pathway analysis of the genes whose expression differed after SNRPB knockout revealed that these genes were related mainly to DNA replication, the mitochondrial matrix, and the defense response against viruses (Figure 5D). To more accurately identify the genes downstream of SNRPB, we overexpressed SNRPB and performed RNA-seq on RNA samples from the overexpressed cells and control 786-O cells to analyze differentially expressed genes. A total of 1023 upregulated genes and 483 downregulated genes were identified (Figure 5B). We used the intersection of the differentially expressed genes from the knockdown and overexpression groups to identify the genes downstream of SNRPB. A total of 7 genes were obtained through intersection. We designed primers for each gene and performed qPCR experiments. The results revealed that the expression of most of these genes was consistent with the sequencing results (Figure 5E–F). After genes with no or small differences were excluded, we selected RDM1 and TRPV1 as candidate downstream genes and verified their expression through western blotting. TRPV1 protein levels were not consistent with its mRNA expression. Consequently, RDM1 was selected as the downstream gene of SNRPB. Interestingly, multiple pathways related to DNA replication were altered after SNRPB knockout, and RDM1 is directly involved in DNA replication (Figure 5C). Western blotting revealed that SNRPB depletion significantly reduced the protein expression of RDM1 in 786-O and 769-P cells, whereas SNRPB overexpression significantly increased the protein expression of RDM1 (Figure 5G–H). These results indicate that RDM1 is a key downstream target of SNRPB in clear cell renal cell carcinoma. To study the regulatory mechanism through which SNRPB regulates the expression of RDM1, we designed primers to analyze the expression of different RDM1 transcripts (Figure 5I). A significant increase was observed in the skipping frequency of exons 4 and 5 of the pre-mRNA of RDM1 (Figure 5I). Additionally, we analyzed the splicing variants of the mRNA transcripts of RDM1 from the Ensembl database. RDM1 has 7 exons and encodes the normal RDM1 protein. When exons 4 and 5 are skipped, the RDM1-212 transcript is produced (Figure 5J). This transcript is degraded through the nonsense-mediated RNA decay (NMD) pathway, thereby decreasing the mRNA and protein expression of RDM1. Given the NMD-regulated expression of the RDM1-212 transcript, we next tested whether inhibition of NMD was sufficient to increase the mRNA level of RDM1. UPF1 is a core protein involved in the NMD mechanism. Compared with shNC-treated cells, the expression of RDM1 increased in 786-O cells following UPF1 downregulation (Figure 5K–L). Moreover, we performed RNA immunoprecipitation (RIP) assays on the extracts from SNRPB-overexpressing 786-O and 769-P cells by using an SNRPB antibody. Compared with that in the immunoglobulin group, the expression of RDM1 in the SNRPB-overexpressing cell precipitate

was significantly enriched (Figure 5M–N), indicating that SNRPB regulates the mRNA splicing of RDM1 by directly binding to RDM1. These data suggest that SNRPB knockout promotes the splicing of RDM1 pre-mRNA into noncoding transcripts that are degraded by NMD.

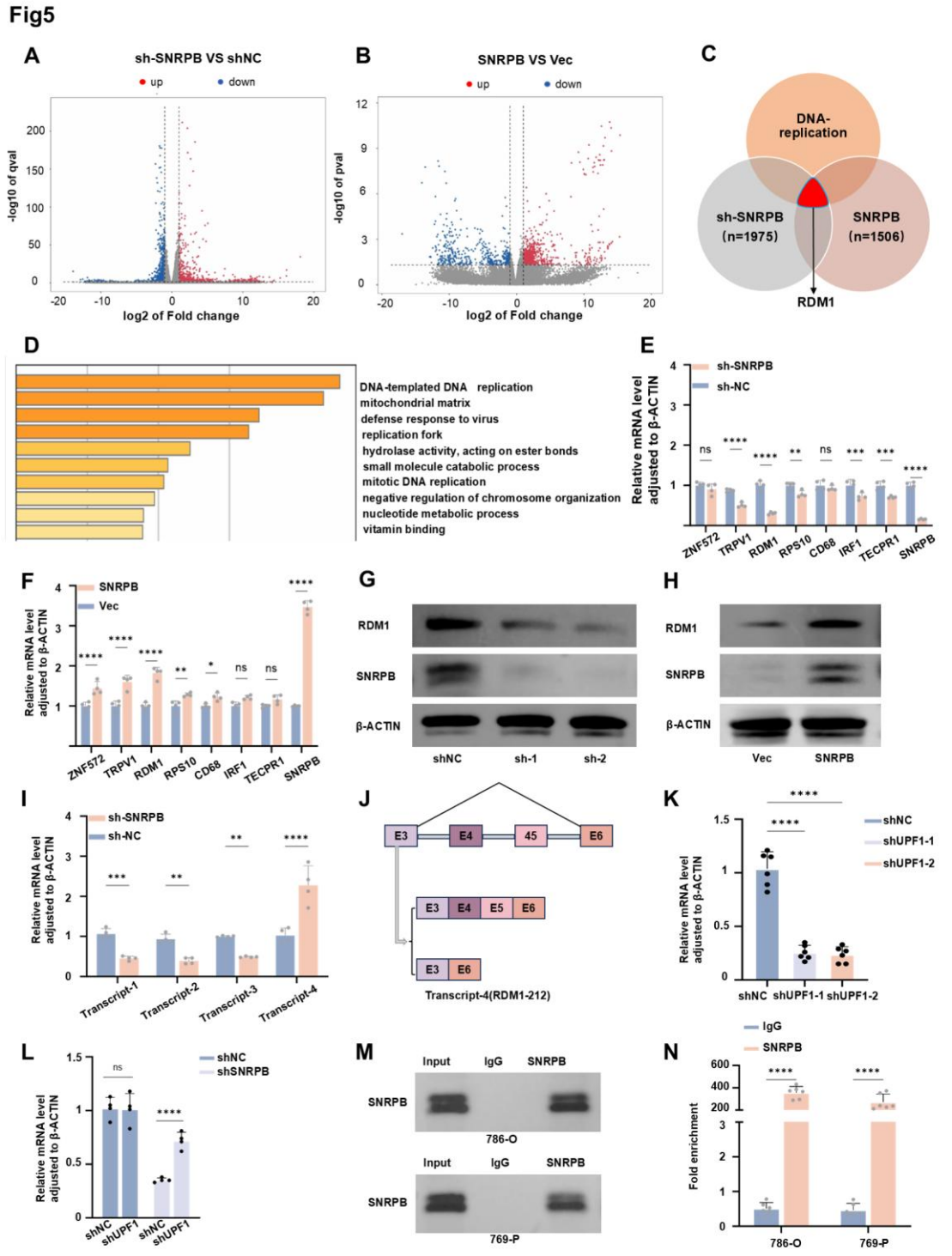


Figure 5. SNRPB regulates the expression of RDM1 through alternative splicing. **A–B:** Volcano plots showing significantly up–and down - regulated genes found in 786–O cells after SNRPB was silenced or overexpressed. **C:** The Venn diagram shows the intersections of differentially expressed genes in 786–O cells after SNRPB knockout and overexpression, as well as genes related to DNA replication. **D:** Enrichment analysis

showing the KEGG pathways of differentially expressed genes in 786 - O cells after SNRPB knockout. **E–F:** qPCR validation of the intersection of differentially expressed genes after SNRPB silencing and overexpression. **G–H:** Western blot analysis of changes in RDM1 expression after SNRPB silencing and overexpression. **I:** Detection of different transcripts of RDM1 in 786–O cells with SNRPB knockdown. **J:** Schematic diagram of the generation of the RDM1 - 212 transcript. **K:** qPCR detection of UPF1 mRNA expression levels in 786–O cells after UPF1 silencing. **L:** qPCR detection of RDM1 mRNA expression levels in 786–O cells after UPF1 silencing. **M:** Co–IP experiments demonstrated successful capture of the SNRPB protein with an antibody. **N:** RIP–qPCR analysis of the relationship between the SNRPB protein and RDM1 mRNA. *$*p < 0.05$, $**p < 0.01$, $****p < 0.0001$*.

RDM1 promotes the in vitro progression of clear cell renal cell carcinoma

To investigate the functional role of RDM1 in clear cell renal cell carcinoma, shRNA targeting RDM1 and overexpression plasmids were designed. In 786-O and 769-P cells, the knockdown efficiency was verified at the mRNA and protein levels (Figure 6A–B). Then, functional analyses were performed to evaluate the effects of RDM1 gene knockout on the phenotypes of clear cell renal cell carcinoma cells. The results of the CCK-8 assay revealed that, compared with that of the shNC group, the proliferation of clear cell renal cell carcinoma cells was significantly reduced after RDM1 was silenced (Figure 6C), while the proliferation of clear cell renal cell carcinoma cells was significantly enhanced after RDM1 overexpression (Figure 6D). The EdU experiment further confirmed these results (Figure 6E–F). Transwell (Figure 6G–H) and wound healing (Figure 6I, Figure S2A–B) analyses consistently revealed that the invasion and migration abilities of clear cell renal cell carcinoma cells significantly decreased after RDM1 gene knockout, whereas these abilities significantly increased after RDM1 overexpression. Flow cytometry was performed to analyze cell apoptosis and study the effect of RDM1 on cell survival. RDM1 gene knockout significantly increased the apoptosis rates of 786-O and 769-P cells, whereas RDM1 overexpression significantly reduced the apoptosis rates(Figure 6J–K,Figure S2C–D).

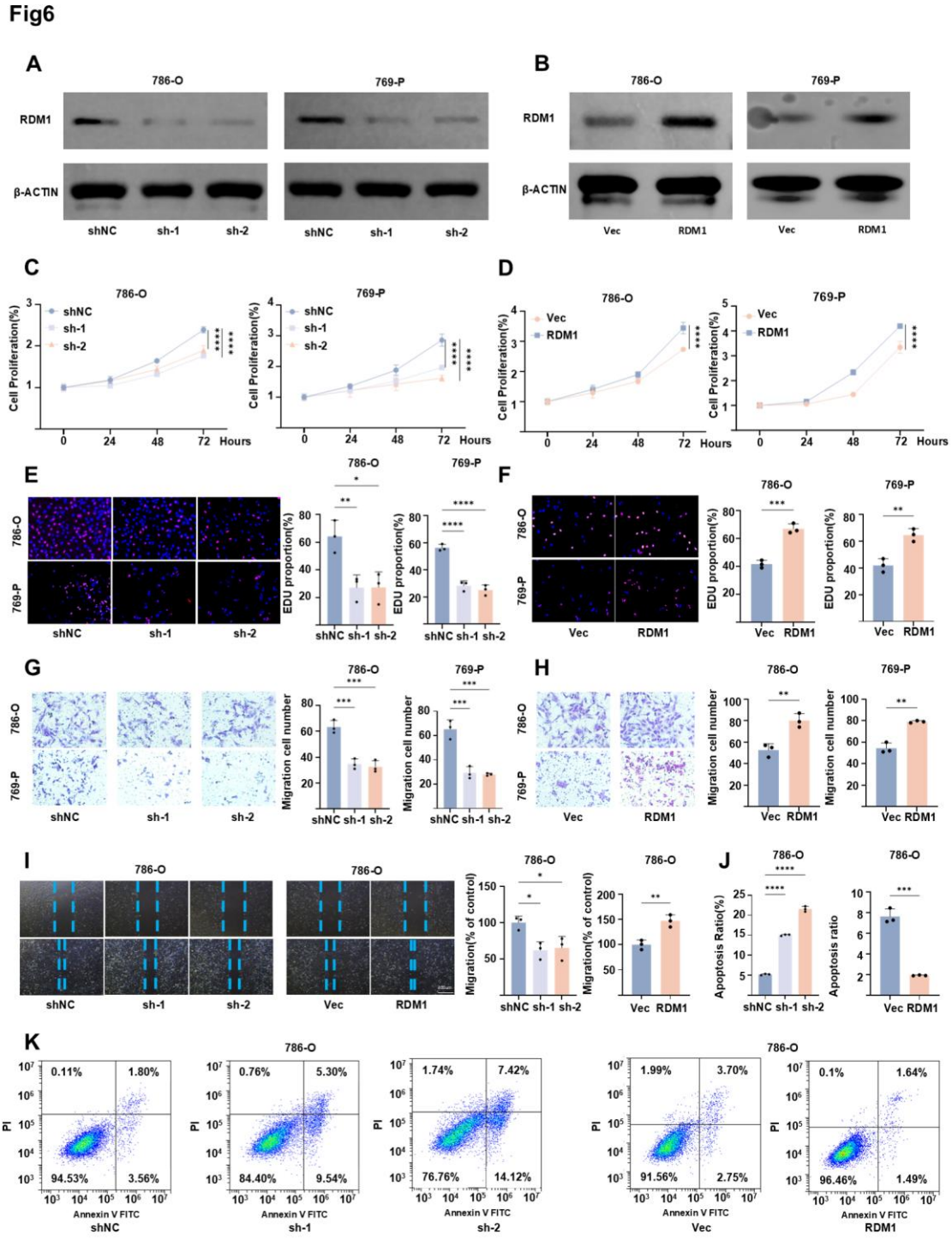


Figure 6. RDM1 silencing inhibits the proliferation and motility of clear–cell renal carcinoma cells in vitro. **A–B:** Western blotting validation of the efficiency of SNRPB knockdown and overexpression in 786–O and 769–P cells. **C–D:** CCK–8 assay to detect the effect of RDM1 knockdown and overexpression on cell viability. **E–F:** EDU assay to detect the effect of RDM1 knockdown and overexpression on cell proliferation. **G–H:** Transwell assay to detect the effect of RDM1 knockdown and overexpression on the invasive ability of clear - cell renal carcinoma cells. **I:** Scratch test to detect the effect of RDM1 knockdown and overexpression on the migratory ability of 786 - O cells. **J–K:** Flow

cytometry was used to quantitatively detect the effect of RDM1 knockdown and overexpression on the apoptosis rate of 786–O cells. *$*p < 0.05$, **$p < 0.01$, ***$p < 0.001$, ****$p < 0.0001$*.

Effects of RDM1 gene overexpression on the oncogenic phenotype of SNRPB in clear cell renal cell carcinoma

To verify the biological function of RDM1 in clear cell renal cell carcinoma cells, we overexpressed RDM1 in SNRPB-knockout 786-O and 769-P cells (Figure 7A). RDM1 overexpression restored the SNRPB knockout-induced decrease in cell proliferation ability in both cells (Figure 7B–D). Similarly, transient introduction of the RDM1 overexpression plasmid into the SNRPB-knockout 786-O and 769-P cells restored the SNRPB knockout-induced weakening of cell invasion and migration abilities (Figure E–G, Figure I). The overexpression of RDM1 in 786-O and 769-P cells also partially reversed the SNRPB knockout-induced increase in apoptosis (Figure H, J). Therefore, RDM1 is a key downstream target that mediates the oncogenic effect of SNRPB in clear cell renal cell carcinoma cells.

Fig7

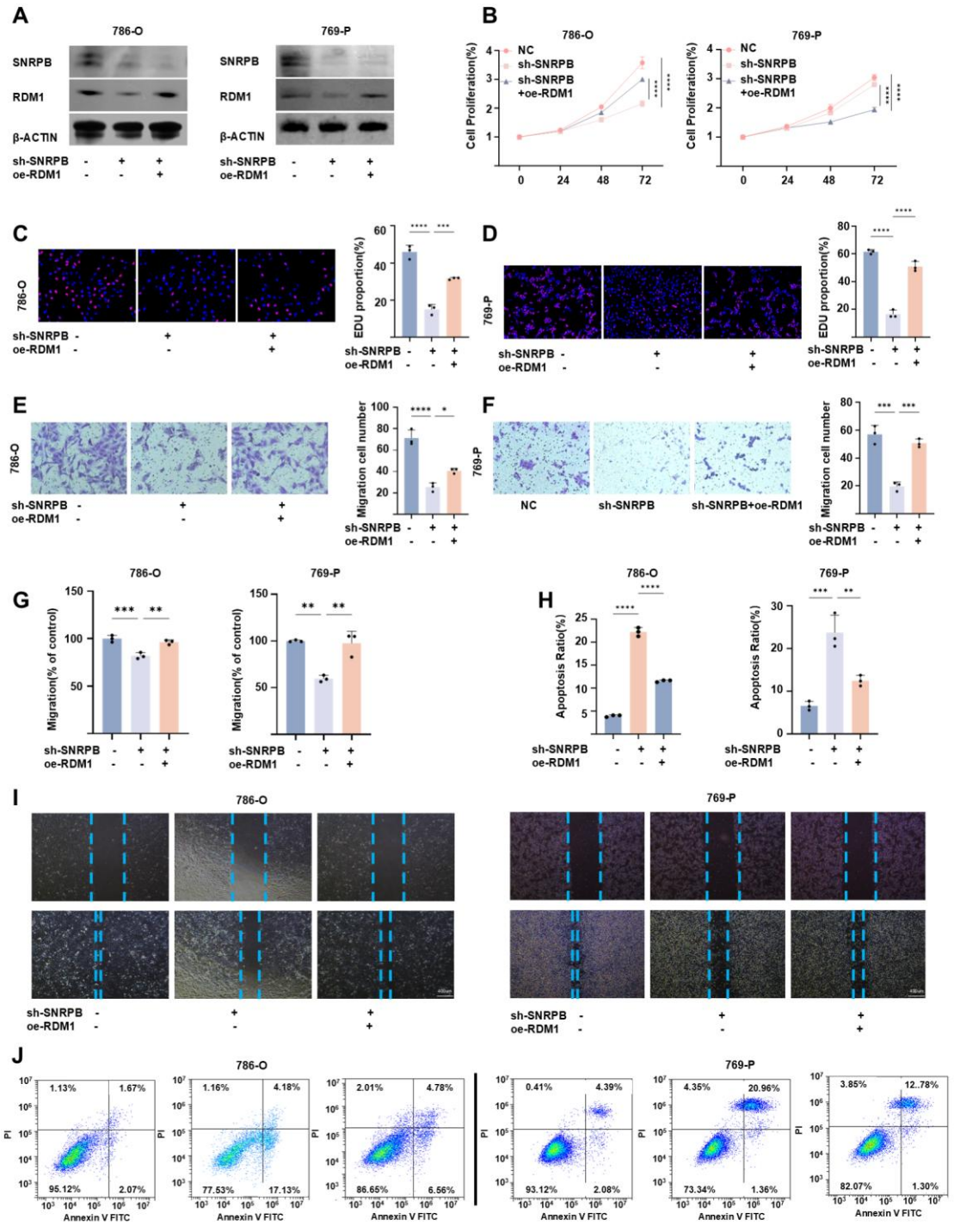


Figure 7. Overexpression of the RDM1 gene can partially reverse the inhibitory effect of SNRPB silencing on the proliferation and motility of renal carcinoma cells cultured in vitro. **A:** Western blotting analysis of the effect of NC, shSNRPB, shSNRPB + oeRDM1 on the expression of SNRPB and RDM1 in 786–O and 769–P cells. **B:** CCK–8 colorimetric assay to detect the effect of NC, shSNRPB, shSNRPB + oeRDM1 on the proliferation of 786–O and 769–P cells. **C–D:** EDU assay to detect the effect of NC, shSNRPB, shSNRPB + oeRDM1 on the proliferation of 786–O and 769–P cells. **E–F:** Transwell assay to detect the effect of NC, shSNRPB, shSNRPB + oeRDM1 on the invasive ability of 786–O and

769–P cells. **G, I:** Scratch test to detect the effect of NC, shSNRPB, shSNRPB + oeRDM1 on the migratory ability of 786–O and 769–P cells. **H, J:** Flow cytometry to detect the effect of NC, shSNRPB, shSNRPB + oeRDM1 on the apoptosis rate of 786 - O and 769 - P cells. **p < 0.05, **p < 0.01, ***p < 0.001, ****p < 0.0001*.

RDM1 affects the malignant behavior of tumor cells by regulating the DNA damage repair ability of cells

As the function of RDM1 itself is related to DNA damage repair, we verified the effect of RDM1 knockdown on the DNA damage repair ability of clear-cell renal cell carcinoma cells through a comet assay and γ-H2AX fluorescent foci. Comet assays revealed that, compared with that in the NC group, DNA damage in 786-O cells was significantly aggravated after SNRPB was silenced, and this situation was significantly improved after RDM1 was overexpressed (Figure 8A–B). We found that after RDM1 was knocked down, compared with those in the control cells, the DNA damage in 786-O cells treated with etoposide for one hour was significantly more severe, and the repair was delayed. After RDM1 was overexpressed in 786-O cells with SNRPB knockdown, the DNA damage repair ability of the cells significantly improved (Figure 8C–D). We subsequently conducted an animal experiment. Six-week-old nude mice were divided into three groups—NC, shSNRPB, and shSNRPB+oeRDM1—and corresponding subcutaneous xenograft tumors were constructed. Compared with those in the control group, the volume and weight of tumors in the SNRPB knockdown group were significantly lower, and the tumor volume and weight increased significantly in the group in which RDM1 was overexpressed (Figure 8E–H). Furthermore, after 786-O cells were treated with 10 μM olaparib and subjected to the CCK-8 assay, the survival rate of renal cancer cells transfected with shSNRPB alone was significantly lower than that of cells transfected with the RDM1 overexpression plasmid (Figure 8I). Therefore, RDM1 may affect the malignant behavior of tumor cells by increasing their ability to repair DNA damage.

Fig8

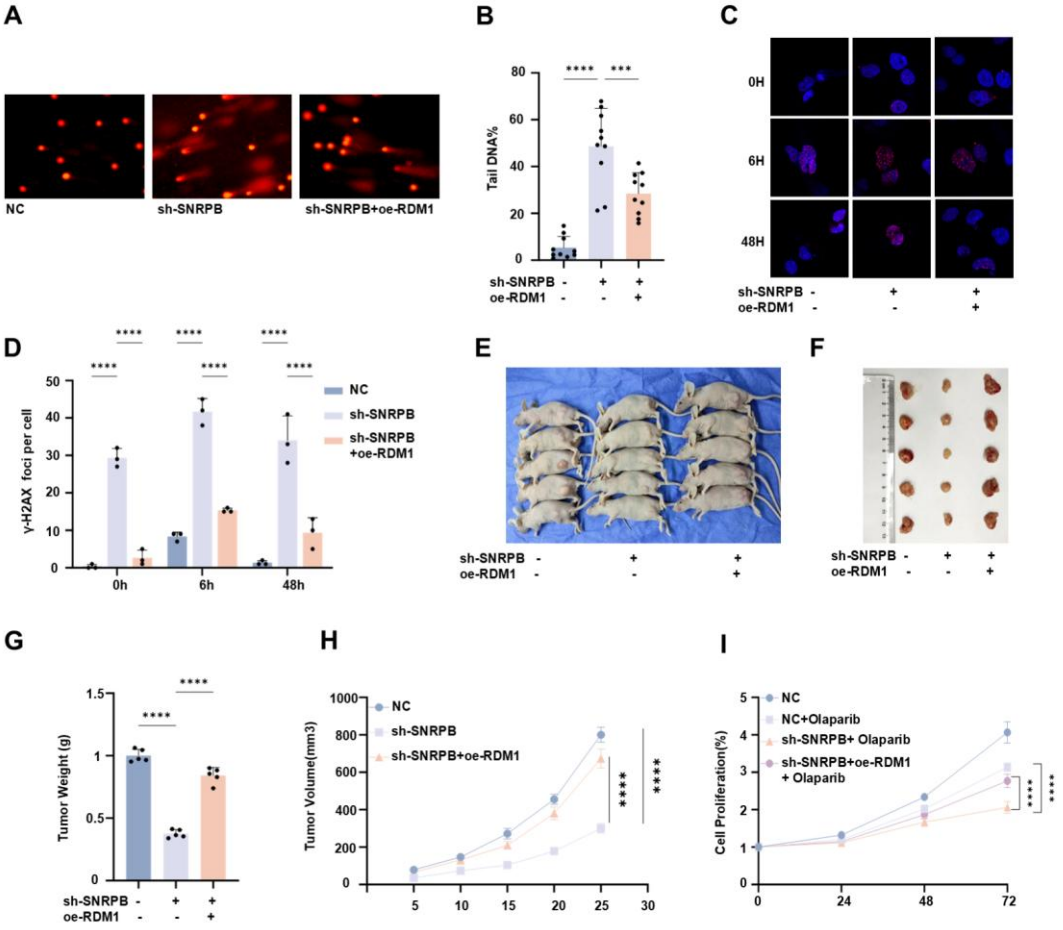


Figure 8. Overexpression of RDM1 can partially restore the DNA damage in 786–O cells caused by SNRPB silencing. **A–B:** Comet assay showed that overexpression of RDM1 can partially restore the DNA damage in 786–O cells caused by SNRPB silencing. **C–D:** Immunofluorescence detection of the formation of γ-H2AX foci in 786-O cells at different time points after treatment with etoposide for 1 hour in the NC group, sh–SNRPB group, and sh - SNRPB + oe - RDM1 group. **E–F:** Lentiviruses encoding NC–shRNA, sh–SNRPB, and sh–SNRPB + oe–RDM1 were used to infect 786–O cells, which were then subcutaneously injected into nude mice. Representative images of subcutaneous xenograft tumors are shown. **G–H:** Tumor weight and growth of renal cell carcinoma xenografts over 25 days. **I:** CCK - 8 assay to detect the proliferation of 786–O cells after 72 h of treatment in the NC group, NC + Olaparib group, sh–SNRPB + Olaparib group, and sh–SNRPB + oe–RDM1 + Olaparib group. ****p < 0.001, ****p < 0.0001*.

Fig9

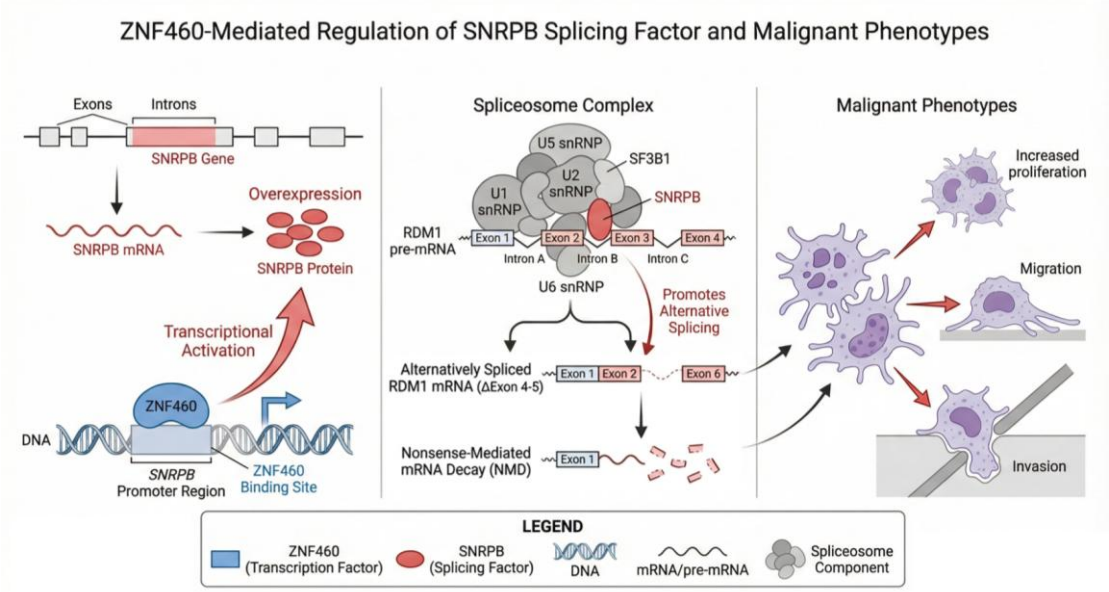


Figure 9. Schematic diagram of the mechanism by which the ZNF460–SNRPB–RDM1 axis affects the phenotypes of renal cancer cells.

FigS1

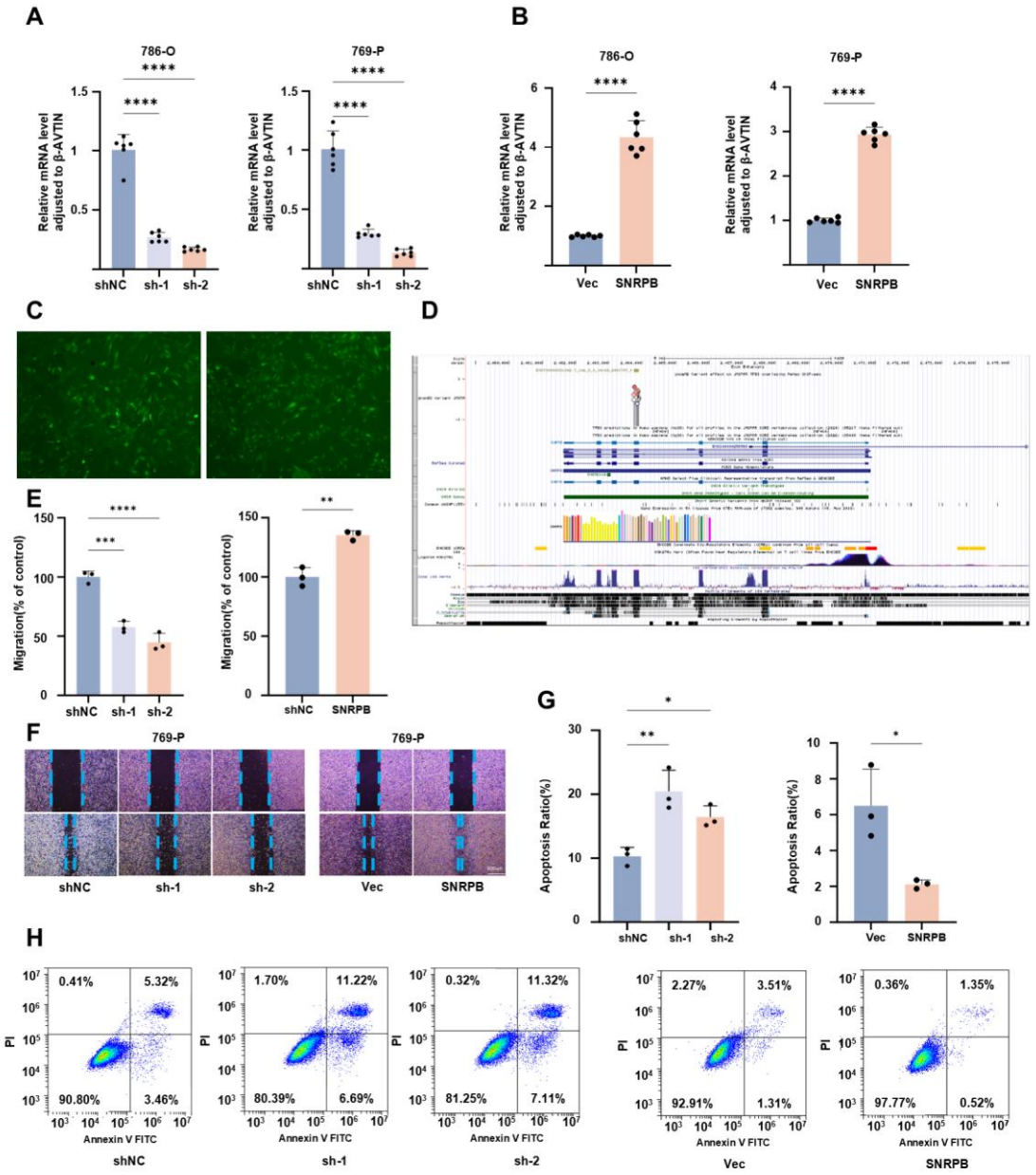


Figure S1. **A–B:** Verification of the RNA level of SNRPB after its knockdown. **C:** Construct a stable transfected 786-O cell line of sh-SNRPB. **D:** Screenshot of the JASPAR website predicting the transcription factor ZNF460. **E–F:** Scratch test to detect the effect of SNRPB knockdown and overexpression on the migration ability of 769–O cells.**G–H:** Flow cytometry to quantitatively detect the effect of SNRPB knockdown and overexpression on the apoptosis rate of 769–P cells. **p < 0.05,**p < 0.01, ***p < 0.001, ****p < 0.0001*.

FigS2

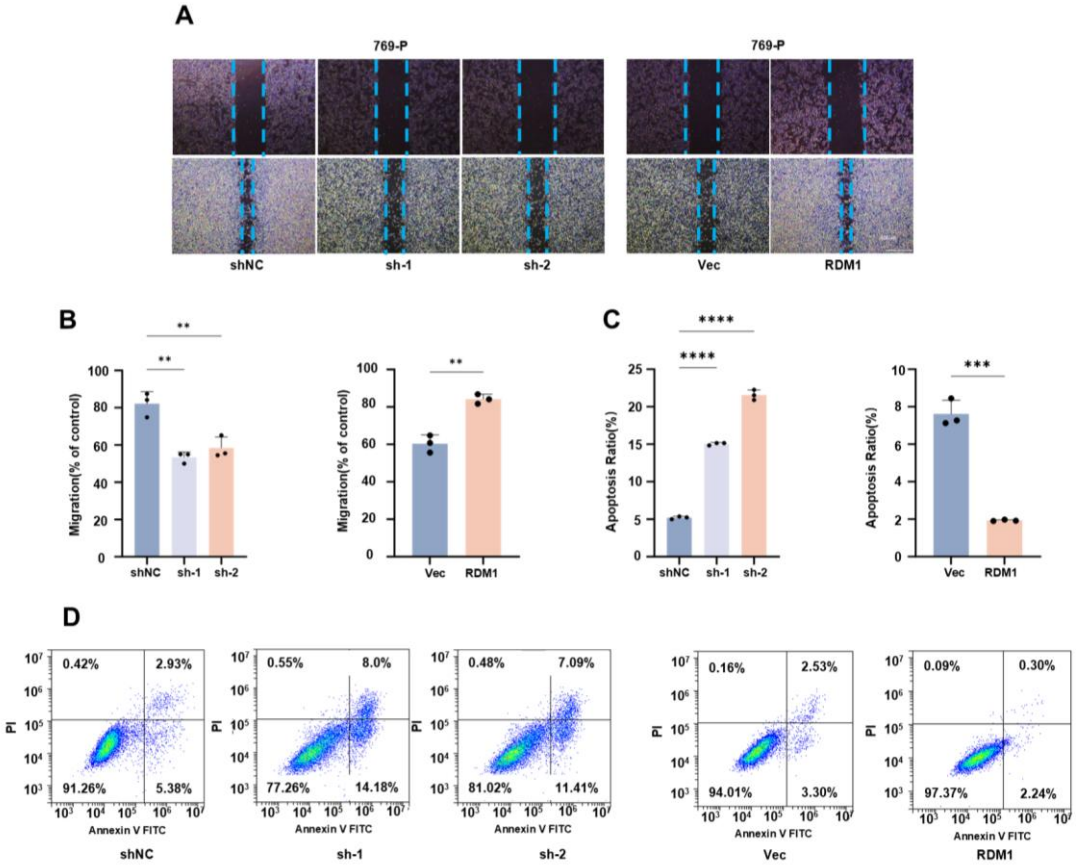


Figure S2. **A–B:** Scratch test to detect the effect of RDM1 knockdown and overexpression on the migration ability of 769-O cells. **C–D:** Flow cytometry to quantitatively detect the effect of RDM1 knockdown and overexpression on the apoptosis rate of 769–P cells. **p < 0.01*, ****p < 0.001*, *****p < 0.0001*.

Discussion

The molecular pathogenesis of clear cell renal cell carcinoma (ccRCC) extends beyond the well-characterized VHL–HIF axis(18-20), involving complex alterations in gene expression and posttranscriptional regulation. In this study, we identified the spliceosome component SNRPB as a novel oncogenic driver in ccRCC. SNRPB was found to be frequently overexpressed in ccRCC tissues and its elevated expression was associated with advanced tumor stage and poor patient prognosis. Functionally, knockdown of SNRPB significantly attenuated the malignant phenotypes of ccRCC cells, including proliferation, invasion, and antiapoptotic ability. Most importantly, we mechanistically revealed that SNRPB plays an oncogenic role mainly by disrupting the alternative splicing of the key factor RDM1 in the DNA damage response, leading to genomic instability and tumor progression.

Our findings are consistent with those of a large body of existing research indicating that spliceosome proteins are key factors in the carcinogenesis of various cancer types. USP39, a component of the spliceosome, is abnormally highly expressed in high-grade serous ovarian cancer (HGSOC) and is associated with poor prognosis. USP39 can promote tumor growth in vivo(21). In chronic lymphocytic leukemia, SF3B1 mutations are associated with more aggressive

disease and shorter survival(22). In uveal melanoma and prolactinoma, SF3B1 mutations are also associated with specific clinicopathological features and poor prognosis(23, 24), respectively. In pancreatic cancer, mutant p53 promotes the abnormal inclusion of cytosine-rich exons in RAS GTPase-activating proteins (GAPs) by upregulating the expression of the splicing regulator hnRNPK, generating GAP isoforms that lose membrane localization function, thereby alleviating the inhibition of KRAS and enhancing its carcinogenic activity(25). In triple-negative breast cancer, knockdown of the spliceosome core protein SNRPD1 induces doxorubicin resistance, suggesting its role in maintaining chemotherapy sensitivity(26).

This study clarified the oncogenic role of SNRPB in clear cell renal cell carcinoma (ccRCC). The potent tumor-suppressive effect observed after SNRPB knockdown highlights its potential as a key dependency factor for ccRCC cell survival, indicating that it is a major regulator of tumorigenesis rather than a passive bystander. SNRPB is highly expressed in non-small cell lung cancer (NSCLC) and functions as an oncogene. Moreover, SNRPB negatively regulates cisplatin resistance in non-small cell lung cancer cells. SNRPB knockdown can significantly reduce cisplatin-induced growth inhibition, cell cycle arrest, and apoptosis in H1299 cells(27). In ovarian cancer, the expression of SNRPB is significantly increased and can significantly promote the proliferation and invasion of ovarian cancer cells(15). In osteosarcoma, SNRPB promotes the transcription of ribonucleotide reductase subunit M2 through E2F transcription factor 1, thereby promoting the malignant phenotype of cells(28). In hepatocellular carcinoma (HCC), SNRPB promotes the progression of HCC by regulating the FOXM1–CCNB1 axis and lipid metabolism and may be a potential therapeutic target for enhancing the chemotherapy sensitivity of patients with HCC(29).

RDM1 is a protein containing an RNA recognition motif (RRM) that was first identified in vertebrates and initially attracted attention due to its role in the cellular response to the anticancer drug cisplatin(30). Subsequent studies have shown that RDM1 plays a crucial role in DNA double - strand break repair and homologous recombination(31, 32). RDM1 is one of the core components of the RNA - mediated DNA methylation (RdDM) pathway and is essential for maintaining transposon silencing and genomic stability(33-35). In lung adenocarcinoma, breast cancer, and neuroblastoma, the expression of RDM1 is significantly upregulated, and its high expression is associated with poor clinical prognosis(36-38). Our data indicate that the overexpression of SNRPB is associated with abnormal splicing of RDM1 precursor mRNA. Silencing SNRPB can promote the skipping of two key exons of RDM1, resulting in transcripts susceptible to nonsense - mediated mRNA decay (NMD) and thus reducing the expression level of RDM1, leading to a decrease in the level of functional RDM1 protein. RDM1 is a key factor in the homologous recombination repair (HRR) pathway and contributes to the repair of DNA double - strand breaks (DSBs). In our rescue experiments, we observed an increase in γ-H2AX focus formation and enhanced sensitivity to DNA - damaging agents such as etoposide in cells with low SNRPB expression, and overexpression of RDM1 could rescue this outcome. Therefore, we propose a therapeutic strategy targeting SNRPB. Knocking down SNRPB→Reducing RDM1 protein →Genomic instability→Increased sensitivity to DNA - damaging drugs. The discovery of this axis has important clinical implications. First, the strong correlation between SNRPB expression and poor prognosis suggests that it may serve as a novel biomarker for risk stratification in patients with ccRCC. Second, more intriguingly, directly targeting the spliceosome mechanism itself may be a potential therapeutic approach for clear - cell renal cell carcinoma. The efficacy of small -

molecule inhibitors targeting spliceosome components can be evaluated in ccRCC models with high SNRPB expression.

In recent years, research has revealed that many cancer cells exhibit unique vulnerabilities to perturbations in spliceosome function, which has given rise to the emerging anticancer strategy of “targeted spliceosome therapy”(39, 40). Recent studies have shown that targeted spliceosome therapies (STTs) can trigger a “virus mimicry” effect. Splicing errors lead to the accumulation of intron-containing transcripts in the cytoplasm and the formation of double-stranded RNA (dsRNA), thereby activating the intracellular antiviral signaling pathway and inducing type I interferon responses and apoptosis(41, 42). In immunocompetent models, this cell–intrinsic immune activation can further trigger an adaptive immune response, converting “immune–cold” tumors into an “immune–hot” state, providing a theoretical basis for combination immunotherapy(41, 43). Targeting the spliceosome has become a promising strategy in cancer treatment. This approach is based on the unique dependence of cancer cells on splicing integrity, which stems from high-frequency spliceosome-driven mutations or splicing stress induced by oncogenic signals. The mechanism of action extends from direct splicing interference and cytotoxicity to the activation of the endogenous antiviral immune pathway, thus connecting targeted therapy with tumor immunity. Despite challenges such as selectivity and toxicity, through precise patient stratification, rational combination strategies, and the development of new targets for nonclassical spliceosome-related functions, targeted spliceosome therapies are expected to serve as new treatment options for cancer patients who currently lack effective therapies.

Despite these findings, our study has several limitations. Although RDM1 is the main effector, SNRPB, as a core spliceosome protein, may regulate a series of downstream targets. Performing a more comprehensive “splicing signature” analysis using RNA sequencing after SNRPB regulation helps to elucidate its oncogenic function.

In summary, our work revealed a previously unrecognized oncogenic pathway in ccRCC that is driven by SNRPB overexpression. We provide compelling evidence that SNRPB promotes tumorigenesis by inducing the aberrant splicing of RDM1, ultimately affecting DNA damage responses and genomic stability. These findings not only deepen our understanding of ccRCC biology but also reveal SNRPB and associated RDM1 deficiency as attractive biomarkers and therapeutic targets, providing new hope in the fight against this deadly malignancy.

References

1. Young M, Jackson-Spence F, Beltran L, Day E, Suarez C, Bex A, et al. Renal cell carcinoma. Lancet. 2024;404(10451):476-91.

2. Rose TL, Kim WY. Renal Cell Carcinoma: A Review. JAMA. 2024;332(12):1001-10.

3. Abah MO, Ogenyi DO, Zhilenkova AV, Essogmo FE, Ngaha Tchawe YS, Uchendu IK, et al. Innovative Therapies Targeting Drug-Resistant Biomarkers in Metastatic Clear Cell Renal Cell Carcinoma (ccRCC). Int J Mol Sci. 2024;26(1).

4. Bianchi N, Ancona P, Aguiari G. Molecular Mechanisms of Drug Resistance in Clear Cell Renal Cell Carcinoma. Cancers (Basel). 2025;17(10).

5. Brugarolas J. Molecular genetics of clear-cell renal cell carcinoma. J Clin Oncol. 2014;32(18):1968-76.

6. Kanno T, Kamba T, Yamasaki T, Shibasaki N, Saito R, Terada N, et al. JunB promotes cell invasion and angiogenesis in VHL-defective renal cell carcinoma. Oncogene. 2012;31(25):3098-110.

7. Staller P. Genetic heterogeneity and chromatin modifiers in renal clear cell carcinoma. Future Oncol. 2010;6(6):897-900.
8. Gao W, Li W, Xiao T, Liu XS, Kaelin WG, Jr. Inactivation of the PBRM1 tumor suppressor gene amplifies the HIF-response in VHL-/- clear cell renal carcinoma. Proc Natl Acad Sci U S A. 2017;114(5):1027-32.
9. Choi S, Cho N, Kim EM, Kim KK. The role of alternative pre-mRNA splicing in cancer progression. Cancer Cell Int. 2023;23(1):249.
10. Rahman MA, Krainer AR, Abdel-Wahab O. SnapShot: Splicing Alterations in Cancer. Cell. 2020;180(1):208- e1.
11. Kitamura K, Nimura K. Regulation of RNA Splicing: Aberrant Splicing Regulation and Therapeutic Targets in Cancer. Cells. 2021;10(4).
12. Bonnal SC, Lopez-Oreja I, Valcarcel J. Roles and mechanisms of alternative splicing in cancer - implications for care. Nat Rev Clin Oncol. 2020;17(8):457-74.
13. Zhao H, Wu N, Wei G, Zhang H, Ren T, Yi J, et al. Alternative splicing regulation by tumor suppressing subtransferable candidate 4: a pathway to tumor suppression. Front Immunol. 2024;15:1474527.
14. Wang Z, Yang X, Liu C, Li X, Zhang B, Wang B, et al. Acetylation of PHF5A Modulates Stress Responses and Colorectal Carcinogenesis through Alternative Splicing-Mediated Upregulation of KDM3A. Mol Cell. 2019;74(6):1250-63 e6.
15. Li Y, Chen Z, Peng J, Yuan C, Yan S, Yang N, et al. The splicing factor SNRPB promotes ovarian cancer progression through regulating aberrant exon skipping of POLA1 and BRCA2. Oncogene. 2023;42(31):2386-401.
16. Li Y, Chen Z, Xiao H, Liu Y, Zhao C, Yang N, et al. Targeting the splicing factor SNRPB inhibits endometrial cancer progression by retaining the POLD1 intron. Exp Mol Med. 2025;57(2):420-35.
17. Zhu L, Zhang X, Sun Z. SNRPB promotes cervical cancer progression through repressing p53 expression. Biomed Pharmacother. 2020;125:109948.
18. Grampp S, Platt JL, Lauer V, Salama R, Kranz F, Neumann VK, et al. Genetic variation at the 8q24.21 renal cancer susceptibility locus affects HIF binding to a MYC enhancer. Nat Commun. 2016;7:13183.
19. Greene CJ, Sharma NJ, Fiorica PN, Forrester E, Smith GJ, Gross KW, et al. Suppressive effects of iron chelation in clear cell renal cell carcinoma and their dependency on VHL inactivation. Free Radic Biol Med. 2019;133:295-309.
20. Zhang X, Li S, He J, Jin Y, Zhang R, Dong W, et al. TET2 Suppresses VHL Deficiency-Driven Clear Cell Renal Cell Carcinoma by Inhibiting HIF Signaling. Cancer Res. 2022;82(11):2097-109.
21. Wang S, Wang Z, Li J, Qin J, Song J, Li Y, et al. Splicing factor USP39 promotes ovarian cancer malignancy through maintaining efficient splicing of oncogenic HMGA2. Cell Death Dis. 2021;12(4):294.
22. Wan Y, Wu CJ. SF3B1 mutations in chronic lymphocytic leukemia. Blood. 2013;121(23):4627-34.
23. Alsafadi S, Houy A, Battistella A, Popova T, Wassef M, Henry E, et al. Cancer-associated SF3B1 mutations affect alternative splicing by promoting alternative branchpoint usage. Nat Commun. 2016;7:10615.
24. Li C, Xie W, Rosenblum JS, Zhou J, Guo J, Miao Y, et al. Somatic SF3B1 hotspot mutation in prolactinomas. Nat Commun. 2020;11(1):2506.

25. Escobar-Hoyos LF, Penson A, Kannan R, Cho H, Pan CH, Singh RK, et al. Altered RNA Splicing by Mutant p53 Activates Oncogenic RAS Signaling in Pancreatic Cancer. Cancer Cell. 2020;38(2):198-211 e8.
26. Dai X, Cai L, Zhang Z, Li J. SNRPD1 conveys prognostic value on breast cancer survival and is required for anthracycline sensitivity. BMC Cancer. 2023;23(1):376.
27. Liu N, Chen A, Feng N, Liu X, Zhang L. SNRPB is a mediator for cellular response to cisplatin in non-small-cell lung cancer. Med Oncol. 2021;38(5):57.
28. Shi Y, Wang Z, Zhang J, He P, Yang M, Zhao C, et al. Small Nuclear Ribonucleoprotein Polypeptides B and B1 Promote Osteosarcoma Progression via Activating the Ataxia-Telangiectasia Mutated Signaling Pathway through Ribonucleotide Reductase Subunit M2. Am J Pathol. 2024;194(11):2163-78.
29. Jin X, He X, Huang R, Liu Q, Wang L, Bai X, et al. SNRPB/CCNB1 axis promotes hepatocellular carcinoma progression and cisplatin resistance through enhancing lipid metabolism reprogramming. J Exp Clin Cancer Res. 2025;44(1):211.
30. Hamimes S, Arakawa H, Stasiak AZ, Kierzek AM, Hirano S, Yang YG, et al. RDM1, a novel RNA recognition motif (RRM)-containing protein involved in the cell response to cisplatin in vertebrates. J Biol Chem. 2005;280(10):9225-35.
31. Sheng J, Liu K, Sun D, Nie P, Mu Z, Chen H, et al. Association of RDM1 with osteosarcoma progression via cell cycle and MEK/ERK signalling pathway regulation. J Cell Mol Med. 2021;25(16):8039-46.
32. Chen SL, Liu LL, Wang CH, Lu SX, Yang X, He YF, et al. Loss of RDM1 enhances hepatocellular carcinoma progression via p53 and Ras/Raf/ERK pathways. Mol Oncol. 2020;14(2):373-86.
33. Gao Z, Liu HL, Daxinger L, Pontes O, He X, Qian W, et al. An RNA polymerase II- and AGO4-associated protein acts in RNA-directed DNA methylation. Nature. 2010;465(7294):106-9.
34. Law JA, Ausin I, Johnson LM, Vashisht AA, Zhu JK, Wohlschlegel JA, et al. A protein complex required for polymerase V transcripts and RNA- directed DNA methylation in Arabidopsis. Curr Biol. 2010;20(10):951-6.
35. Sasaki T, Lorkovic ZJ, Liang SC, Matzke AJ, Matzke M. The ability to form homodimers is essential for RDM1 to function in RNA-directed DNA methylation. PLoS One. 2014;9(2):e88190.
36. Tong L, Liu J, Yan W, Cao W, Shen S, Li K, et al. RDM1 plays an oncogenic role in human lung adenocarcinoma cells. Sci Rep. 2018;8(1):11525.
37. Xie G, Wu H, Cai W, Chen M, Huang W, Yan W, et al. RDM1 promotes neuroblastoma growth through the RAS-Raf-MEK-ERK pathway. FEBS Open Bio. 2019;9(3):490-7.
38. Chen Y, Sun Z, Zhong T. RDM1 promotes critical processes in breast cancer tumorigenesis. J Cell Mol Med. 2019;23(8):5432-9.
39. Yoshimi A, Abdel-Wahab O. Molecular Pathways: Understanding and Targeting Mutant Spliceosomal Proteins. Clin Cancer Res. 2017;23(2):336-41.
40. Eymin B. Targeting the spliceosome machinery: A new therapeutic axis in cancer? Biochem Pharmacol. 2021;189:114039.
41. Bowling EA, Wang JH, Gong F, Wu W, Neill NJ, Kim IS, et al. Spliceosome-targeted therapies trigger an antiviral immune response in triple-negative breast cancer. Cell. 2021;184(2):384-403 e21.
42. Ishak CA, Loo Yau H, De Carvalho DD. Spliceosome-Targeted Therapies Induce dsRNA Responses. Immunity. 2021;54(1):11-3.
43. Yang H, Beutler B, Zhang D. Emerging roles of spliceosome in cancer and immunity. Protein Cell. 2022;13(8):559-79.

Author Contributions

Zhu Jin and Wang Lixia are co-corrsesponding author, they designed experiments, analysed data and wrote/edited the manuscript. Liu Kang conducts molecular biology experiments, cytology experiments, and animal experiments and performs data analysis. Yao yao conducts bioinformatics analysis.data. Xiang Han collects clinical specimens.. Jiang Chunchao and Wang Yang conducts molecular biology experiment and analyzed the data.

Fundings

Wang Lixia was funded by the Basic Research Program of Jiangsu (BK20251786).

Competing Interests

The authors declare no competing interests.

Ethics Approval and Consent to Participate

Approval for the use of patient samples was granted by the ethical committee of The Second Affiliated Hospital of Soochow University andall samples were collected with informed consent. All methods were performed in accordance with the relevant guidelines and regulations.